Beyond the Rayleigh instability limit for multicharged finite systems: From fission to Coulomb explosion

Isidore Last, Yaakov Levy, and Joshua Jortner*

School of Chemistry, Tel Aviv University, Ramat Aviv, Tel Aviv 69978, Israel

Contributed by Joshua Jortner, April 29, 2002

We address the stability of multicharged finite systems driven by Coulomb forces beyond the Rayleigh instability limit. Our exploration of the nuclear dynamics of heavily charged Morse clusters enabled us to vary the range of the pair potential and of the fissibility parameter, which results in distinct fragmentation patterns and in the angular distributions of the fragments. The Rayleigh instability limit separates between nearly binary (or tertiary) spatially unisotropic fission and spatially isotropic Coulomb explosion into a large number of small, ionic fragments. Implications are addressed for a broad spectrum of dynamics in chemical physics, radiation physics of ultracold gases, and biophysics, involving the fission of clusters and droplets, the realization of Coulomb explosion of molecular clusters, the isotropic expansion of optical molasses, and the Coulomb instability of "isolated" proteins.

The fragmentation of multiply charged finite systems driven by long-range Coulomb forces (1–33) or their analogue (34), i.e., nuclei (1–4), clusters (5–29), droplets (30–33), and optical molasses (34), raises some interesting questions regarding the energetics and dynamics of dissociation. How does a finite system respond to a large excess charge (1–33) or effective charge (34)? What are the topography and topology of the multidimensional energy landscape (4, 35) that guide the system's shape evolution and fragmentation? What are the fragmentation channels and under what conditions are they realized? What is the interplay between fission, i.e., instability toward dissociation, of the finite system into two (or a small number of) fragments and Coulomb explosion (17–29) into a large number $\sim n$ (where n is the number of constituents) of ionic species? On the basis of molecular dynamics simulations of the fragmentation patterns of heavily charged Morse clusters we established that the Rayleigh instability limit (30) separates between nearly binary (or tertiary) spatially unisotropic fission and spatially isotropic Coulomb explosion into a large number of ionic fragments.

The ubiquity of fission phenomena of droplets (30–33), nuclei (1–4), and clusters (5–16) was traditionally described by the liquid drop model (LDM) of Lord Rayleigh (30), Meitner and Frisch (2), and Wheeler and Bohr (1), where a classical charged drop deforms through elongated shapes to form separate droplets. The fissibility parameter $X = E(\text{Coulomb})/2E(\text{surface})$ characterizes the relative contribution of repulsive (Coulomb) and cohesive (surface) energies to the fission barrier, separating between the bound initial states and the fission products. For $X < 1$, thermally activated fission over the barrier prevails. At the Rayleigh instability limit of $X = 1$, the barrier height is zero (1, 30). Many features of nuclear and metal cluster fission go beyond the physics of a classical liquid droplet and require the incorporation of quantum shell structure and dynamics (4, 10). Nevertheless, the simple LDM expression $X = Z^2e^2/16\pi\gamma R^3 = (Z^2/n)/(Z^2/n)_{cr}$ with $(Z^2/n)_{cr} = 16\pi\gamma r_0^3/e^2$ (where γ is the surface tension, Z the total charge, R the system's radius, and r_0 the constituent radius) provided the conceptual framework for the fission of charged finite systems. The LDM accounts for the gross universal features of Coulomb instability of finite systems, with $(Z^2/n)_{cr} \simeq 50$ for nuclei (1–3), $(Z^2/n)_{cr} \simeq 0.40$–0.50 for metal clusters (10), and $(Z^2/n)_{cr} \simeq 0.1$ for hydrogen-bonded clusters (31–33). The values of $(Z^2/n)_{cr}$, which correspond to the Rayleigh instability for the onset of barrierless fission ($X = 1$), reflect on the quantitative difference between the surface properties of nuclear matter held by strong cohesive interactions and of molecular matter held by chemical and van der Waals binding. All of the ubiquitous phenomena of fission were experimentally realized for the fissibility parameter below the Rayleigh instability limit of $X = 1$, i.e., nuclear fission (36), the fission of metal clusters (14, 15), and of hydrogen-bonded clusters (31–33). In all these diversely charged finite systems (with $X < 1$), thermally activated fission is dominated by the geometry and the topology of the potential energy hypersurface (4). Beyond the fissibility limit ($X > 1$), barrierless fission and other dissociative channels can open up, but this barrierless domain was not yet explored. In this context, Coulomb explosion of highly charged clusters and large molecules induced by multielectron ionization in ultraintense, ultrashort laser fields (18–29), as well as the expansion of ultracold optical molasses (34), constitute new dissociative phenomena induced by Coulomb instability of multicharged finite systems or their analogy for finite ultracold gases (34), which were not yet related to fission.

Multicharged Morse Clusters

We shall transcend the Rayleigh instability limit ($X = 1$) for Coulomb instability of large finite systems, demonstrating the prevalence of a qualitatively different fragmentation pattern of Coulomb explosion beyond the Rayleigh instability limit. We explored the fragmentation patterns and dynamics of highly charged Morse clusters by varying the range of the pair potential and of the fissibility parameters. The instability of multicharged Morse clusters directly reflects on covalently or dispersion-bound chemical and biophysical finite systems. We applied classical (constant energy) molecular dynamics simulations to study the stability, decay patterns, and fragmentation dynamics of multicharged clusters $(A^+)_n$ consisting of singly charged A^+ ions (with a mass of 100 atomic mass units), where the total cluster charge is $Z = n$. The interionic pair potential $U(R)$ (Fig. 1) consisted of an attractive Morse potential and a Coulomb repulsion, with $U(R) = DG(G - 2) + Be^2/R$, where $G = \exp[-\alpha(R - R_e)]$, the parameters of the Morse potential being D (dissociation energy), α (range parameter), and R_e (equilibrium pair distance), while $B = 14.385$ eV/Å. The interionic pair potential $U(R)$ is purely repulsive for $D < D_0(\alpha, R_e)$ and exhibits a minimum and a barrier for $D > D_0$ (Fig. 1). Two sets of Morse potential parameters were considered. (i) Short-range Morse potential, with $\alpha = 3\text{Å}^{-1}$ and $R_e = 3$Å, where $\alpha R_e = 9$, so that the interaction between nonneighboring atoms is negligibly small. (ii) Long-range Morse potential, with $\alpha = 1\text{Å}^{-1}$ and $R_e = 2$Å, where $\alpha R_e = 2$ and the contribution of interactions between nonneighboring atoms is of significance. The total potential energy (Fig. 1) of a multicharged $(A^+)_n$ cluster is $E = \Sigma\Sigma_{i<j} U(R_{ij})$, consisting of a repulsive Coulomb component and an

Abbreviation: LDM, liquid drop model.

*To whom reprint requests may be addressed. E-mail: jortner@chemsg1.tau.ac.il.

CHEMISTRY

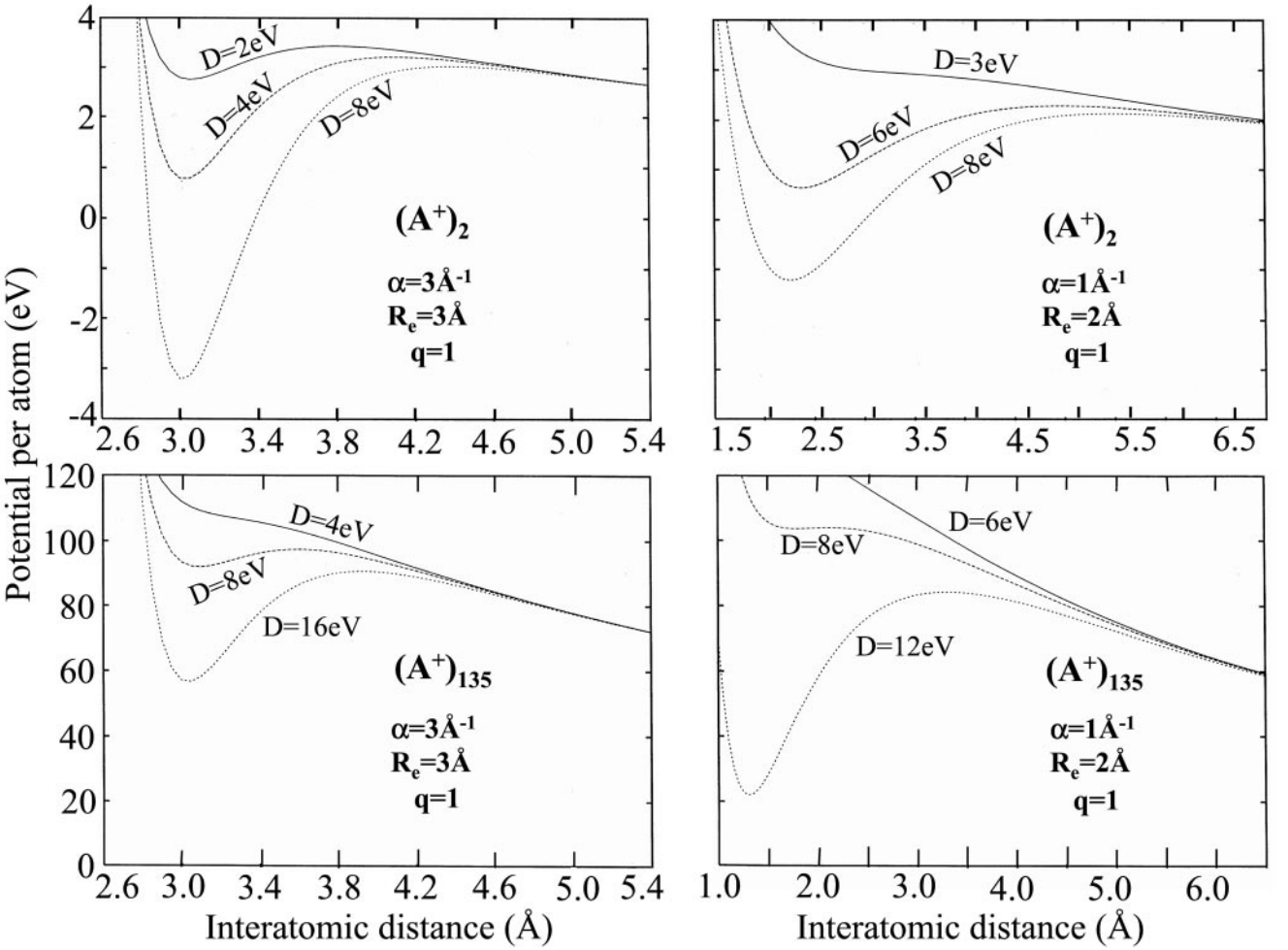

Fig. 1. Pair potentials [*Upper* images, marked $(A^+)_2$] and potential energy landscapes for the radical expansion of $n = 135$ clusters [*Lower* images, marked $(A^+)_{135}$] for the charged Morse clusters. The potential parameters (i) $\alpha = 3\text{Å}^{-1}$, $R_e = 3$Å, and $q = 1$ correspond to the short-range Morse potential, while (ii) $\alpha = 1\text{Å}^{-1}$, $R_e = 2$Å, and $q = 1$ correspond to the long-range Morse potential.

attractive Morse component. The $(A^+)_n$ clusters also exist in a metastable state, with E being higher than the total energy of products in some decay channels but separated from them by barriers (Fig. 1). The equilibrium icosohedral cluster configuration was determined by simulated annealing for the energy minimization. The cluster potential energy for potential parameters (i) and (ii) at the equilibrium configuration is positive, i.e., $E > 0$ (Fig. 1), reflecting on the existence of a metastable state. The cluster energetics at the minimum was analyzed by the LDM, as shown in Fig. 2. The potential energy (per particle) is $E/n = E_M + E_c$, where $E_c = a_c n^{2/3}$ is the Coulomb energy (per particle) while the Morse energy (per particle) is $E_M = E_s + E_v$ and where the surface energy (per particle) is $E_s = a_s n^{-1/3}$, while the interior energy (per particle) is $E_v = -a_v$. Here the parameters a_c, a_s, and a_v are size-independent. The LDM analysis is based on the calculation of E_c, together with the simple relation for the Morse energy $E_M = (E/n) - E_c \equiv a_s n^{-1/3} - a_v$. The size dependence of the potential energy landscapes of the $(A^+)_n$ charged Morse clusters was calculated for short-range Morse potential (i) with $D = 14.2$ eV and for long-range Morse potential (ii) with $D = 9.6$ eV. From the cluster size dependence of E_c and E_M (Fig. 2) we infer that for the short-range Morse potential $a_c = 4.8 \pm 0.1$ eV, $a_v = -80$ eV, and $a_s = 132$ eV, while for the long-range Morse potential $a_c = 10.8 \pm 2$ eV, $a_v = -600$ eV, and $a_s = 1900$ eV. The one-order of magnitude difference

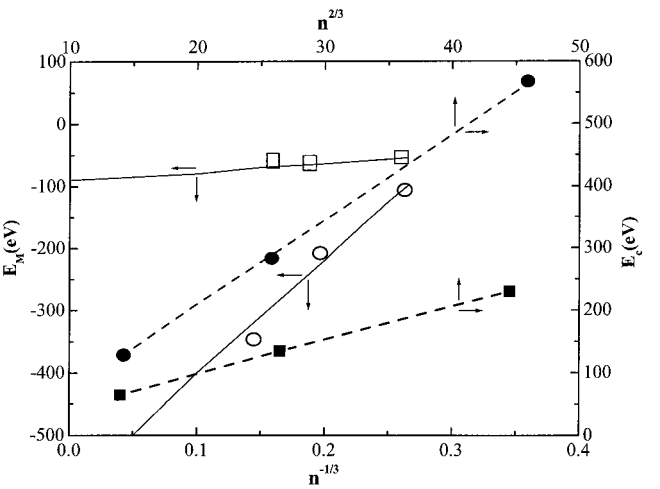

Fig. 2. Analysis of the energetics of icosohedral-charged Morse clusters at their equilibrium configuration by the LDM. The potential parameters are (*i*) short-range Morse potential with $\alpha = 3\text{Å}^{-1}$, $R_e = 3$Å, $D = 14.2$ eV, $q = 1$ and (*ii*) long-range Morse potential with $\alpha = 1\text{Å}^{-1}$, $R_e = 2$Å, $D = 9.6$ eV, $q = 1$. The Coulomb energy per particle is $E_c = a_c n^{2/3}$ [■ for short-range Morse potential (i) and ● for long-range Morse potential (ii)], while the Morse energy per particle is $E_M = a_s n^{-1/3} - a_v$ [□ for short-range potential (i) and ○ for long-range Morse potential (ii)].

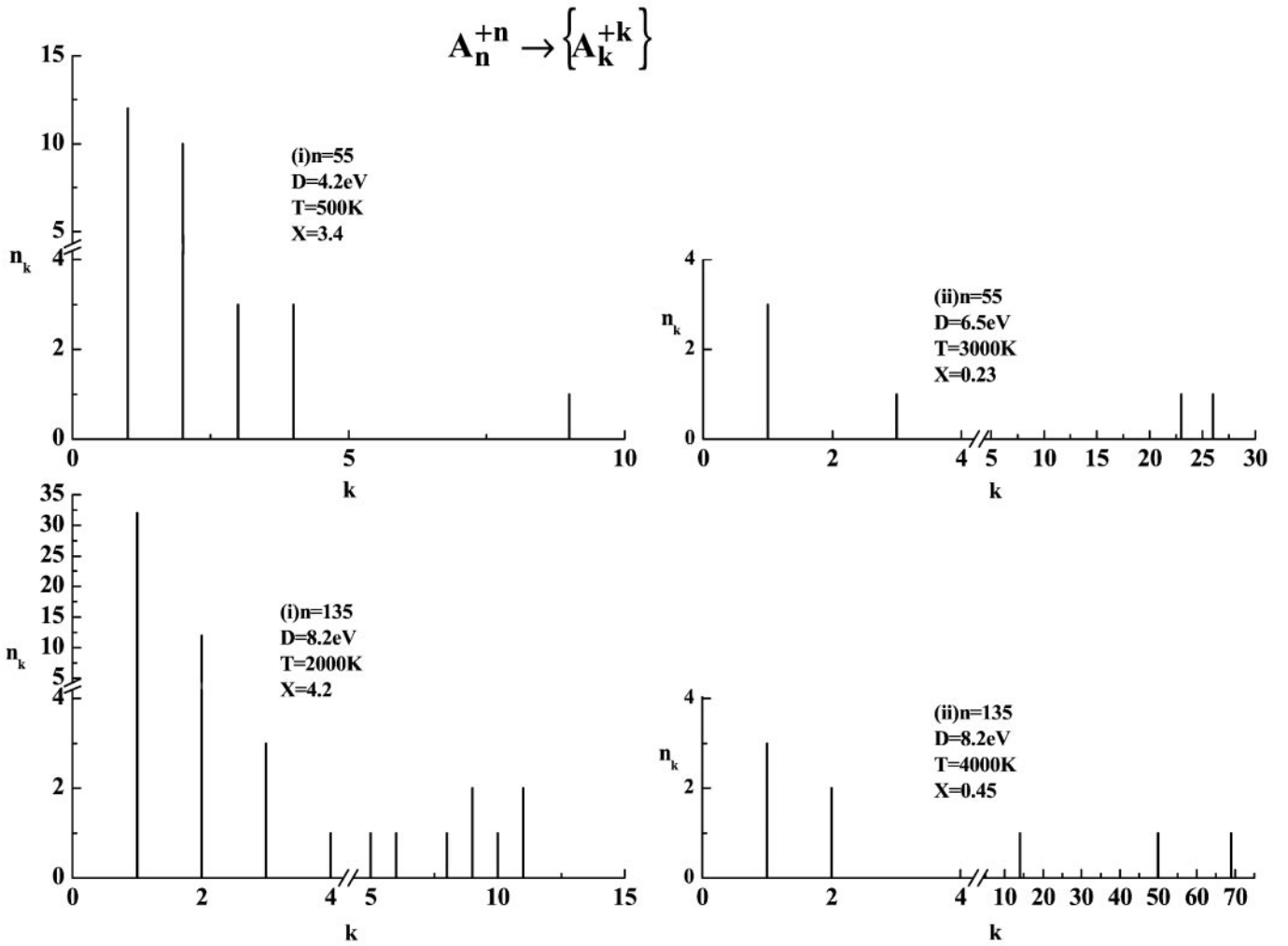

Fig. 3. Fragmentation patterns of charged Morse clusters $\{A_n^{+n}\}$ (n = 55 and 135). The distributions of the ionic fragmentation products $\{A_k^{+k}\}$ are presented in terms of the histograms of the product sizes $\{n_k\}$. (*i*) Short-range Morse potential $\alpha = 3\text{Å}^{-1}$, $R_e = 3$Å, $q = 1$. (*ii*) Long-range Morse potential $\alpha = 1\text{Å}^{-1}$, $R_e = 2$Å, $q = 1$, with the corresponding D and X values marked on the images. Note the fission into a small number of ionic fragments for case (ii) and the Coulomb explosion into a large number of small ionic fragments for case (i).

of the a_s parameters between the long-range and the short-range potentials (while the a_c parameters differ only by a numerical factor of 2 between the two classes of potentials) implies that the fissibility parameter $X = (a_c/a_s)n$ is considerably larger for the short-range potential. The fissibility parameters are $X = 1.81 \cdot 10^{-2} n$ for the short-range Morse potential and $X = 2.82 \cdot 10^{-3} n$ for the long-range Morse potential, which for the cluster size domain $n = 55 - 321$ corresponds to $X \cong 0.1 - 1.0$ for the long-range potential and $X \cong 1 - 7$ for the short-range potential. Our simulations revealed that the qualitative difference in the size domain of the fissibility parameters between the charged long-range and short-range Morse potential implies a qualitatively different fragmentation dynamics driven by Coulomb instability of these two classes of charged Morse clusters.

Dynamics of Fission and Coulomb Explosion

Constant energy molecular dynamics simulations (on time scales of up to 1 ns) were performed for the fragmentation products and dynamics of the icosohedral-charged Morse clusters $A_n^{+n} \rightarrow \{A_k^{+k}\}$ (n = 55, 135, 321), which result in the fragments of charged clusters/ions ($1 \leq k < n$) of sizes $\{n_k\}$ with $\Sigma\, k n_k = n$. As appropriate for thermally activated fragmentation (at least for $X < 1$), the configurationally equilibrated cluster was subjected at $t = 0$ to a temperature jump to a final temperature T. The simulations were performed at the finite temperatures T = 500–10,000 K. Histograms of the ionic products, i.e., n_k vs. k, are presented in Fig. 3. The corresponding values of X were calculated from linear scaling as by the dissociation energies D for Morse potentials (i) and (ii), marked on Fig. 3. For long-range Morse potential (ii), a nearly binary or tertiary cluster fission is exhibited (Fig. 3). The n = 55 cluster (X = 0.23) reveals a nearly symmetric fission, while the n = 135 cluster (X = 0.45) reveals an asymmetric fission into three large clusters (Fig. 3). The fission process is spatially unisotropic, with the deformation of the parent charged cluster occurring via elongation to form separate clusters (Fig. 4). The situation is drastically and qualitatively different for the short-range Morse potential (i) (X = 3.4 for n = 55, and X = 4.2 for n = 135), where the fragmentation involves a large number of small ionic clusters, which manifests Coulomb explosion (Fig. 3). The Coulomb explosion process is spatially isotropic, with the small ionic fragments expanding radially (Fig. 4). The dissociation dynamics were characterized by the (ps) dissociation times, τ_D, which manifest the incubation time for the attainment of the transition state for fragmentation. For the long-range Morse

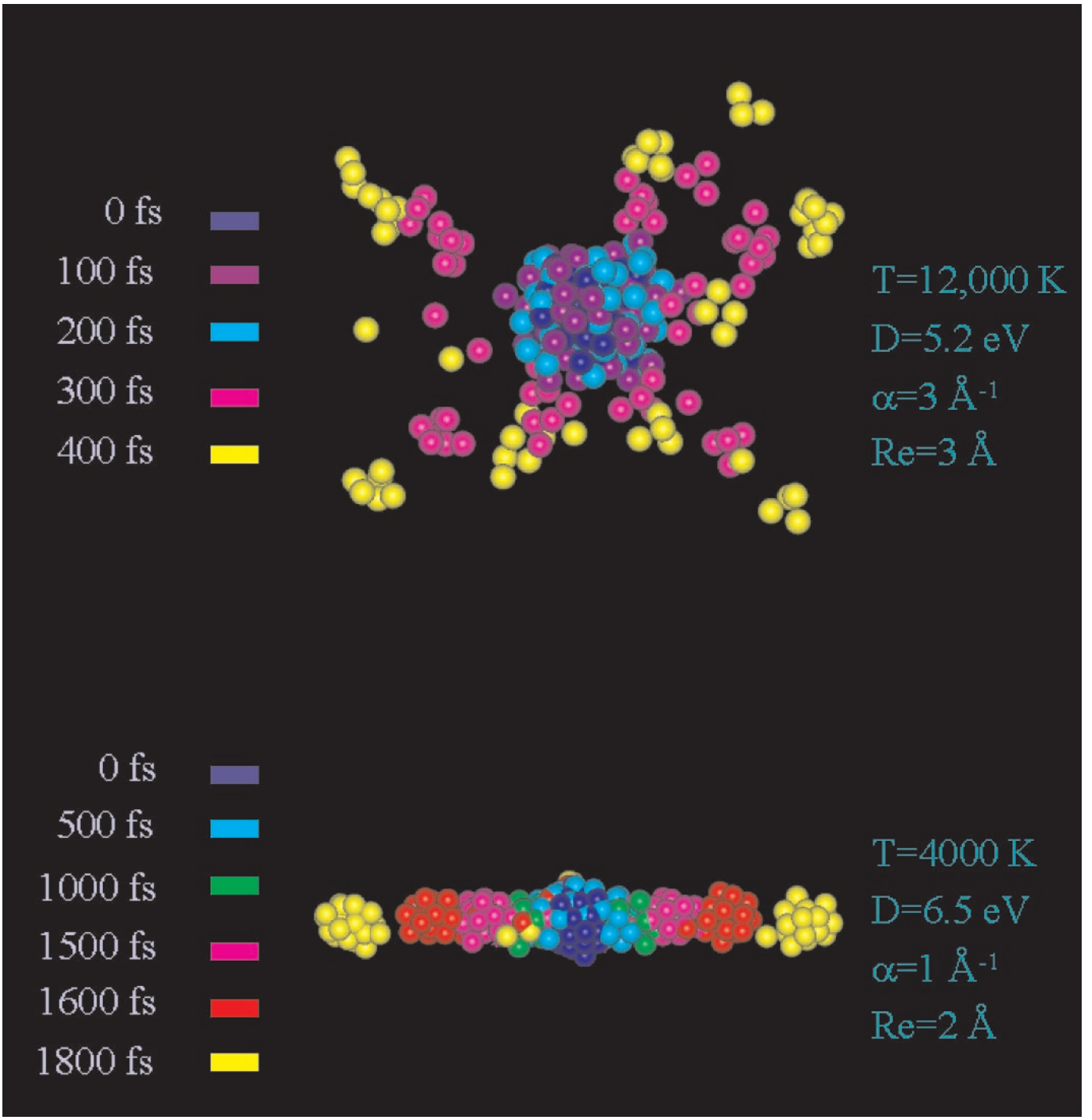

Fig. 4. Superimposed temporal patterns of the fragmentation of highly charged $(A^+)_{55}$ Morse clusters. The potential parameters are marked on the two images. *Upper* panel corresponds to short-range interactions with $X = 4.2$. *Lower* panel corresponds to long-range interactions with $X = 0.23$. The projections of the structures of the disintegrating clusters at different times ($t = 0$–1500 fs) are presented by different colors, marked on each image. The time $t = 0$ corresponds to the T jump to the final temperatures marked on the images. Note the dramatic distinction between the (spatially isotropic) Coulomb explosion (*Upper*) and the (spatially unisotropic) tertiary fission (*Lower*).

potential ($X < 1$), the onset of fission exhibits a weak size dependence, i.e., $\tau_D = 1.0$–0.3 ps for $n = 55$ ($T = 3000$–$10{,}000$ K), and $\tau_D = 0.8$–3.6 ps for $n = 135$ ($T = 2{,}000$–$10{,}000$ K), while for the short-range Morse potential ($X > 1$) the onset of Coulomb explosion manifests a modest decrease of τ_D with increasing the clusters size, i.e., $\tau_D = 1.5$–1.8 ps for $n = 55$ ($T = 1{,}000$–$8{,}000$ K) and $\tau_D = 0.35$–0.5 ps for $n = 135$ ($T = 2{,}000$–$3{,}000$ K).

Epilogue

Our model calculations bridged between (spatially unisotropic) fission and (spatially isotropic) Coulomb explosion of highly charged, strongly bound, molecular clusters demonstrating the prevalence of finite temperature cluster fission into large ionic fragments for $X < 1$, while beyond the fissibility limit, i.e., $X > 1$, Coulomb explosion into elemental-charged constituents provides the dominant dissociation channel. While our results

pertain strictly to covalently bound molecular matter, e.g., molecular clusters, large molecules or biomolecules, droplets, and also to finite ultracold gases (34), some general conclusions are inferred.

The majority of the currently available experimental information on the Coulomb instability of nuclei, of droplets, and of metal clusters pertains to the fission limit ($X < 1$). In the field of nuclear physics, the fissibility parameter is $X \cong 0.7$ for ^{235}U and about $X \cong 0.9$ for the recently discovered $Z = 114$ element (36), while the realization of higher fissibilities, inducing isotropic nuclear Coulomb explosion, requires the nuclear synthesis of heavier elements, which seems to be unattainable at present. For hydrogen-bonded finite systems fission was recorded for droplets below the Rayleigh fissibility limit ($X = 1$) at $X = 0.7$ (T. Leisner, personal communication) and at $X < 1$ (31–33). For multiply charged metal clusters, the maximal value of $X = 0.85 \pm 0.07$ for Na_n^{+z} was recorded (14, 15), although these clusters were not yet produced with a sufficiently large enough charge to overcome the Rayleigh limit. A new fragmentation pattern beyond cluster fission was experimentally recorded (12) for highly charged Na_n clusters produced by collision with multicharged Xe^{20+} ions, with the emission of a large number of singly charged monomers and leaving a single heavy residue of low charge. The production of the light Na^+ ions manifests Coulomb explosion for $X > 1$. Information from Monte-Carlo simulations on evaporation, fission, and multifragmentation of multicharged metal clusters (12) provided information on their Coulomb instability. Our results for molecular matter driven by Coulomb forces, which predict isotropic Coulomb explosion for $X > 1$, concur with the simulation results for the multifragmentation of Na_{70}^{Z+} clusters, which for $Z > 8$ (approximately corresponding to $X > 1.8$) manifest Coulomb explosion into small fragments.

How can the Rayleigh limit for Coulomb instability of finite systems be overcome? This can be accomplished either by a marked enhancement of the repulsive Coulomb energy or by the dramatic reduction of the cohesive surface energy. The increase of E(Coulomb) was experimentally attained for cluster Coulomb explosion induced by ultrashort (1–10 fs) multielectron ionization and nuclear dynamics (10–100 fs) of molecular clusters, e.g., Xe_n, $(D_2)_n$, $(D_2O)_n$ (n = 50–5,000), triggered by ultraintense laser fields (intensity $I = 10^{16}$–10^{18} Wcm^{-2}) (17–29, 37–40). Femtosecond electron dynamics, involving inner and outer cluster ionization (29), strips the cluster atoms/molecules of their outer shell valence electrons, producing highly charged clusters on a time scale shorter than nuclear motion. For these highly charged molecular clusters $X = a(Z^2/n)$, whereupon $X \cong anq_{valence}^2$ [where $a = (Z^2/n)_{cr}^{-1} \approx 1$ for the interparticle van der Waals interaction, and $q_{valence}$ is the valence atomic charge]. The relation $X \gg 1$ is well obeyed for these highly charged molecular clusters, with the dynamics of fragmentation corresponding to the limit of Coulomb explosion. A novel application of this cluster fragmentation mechanism beyond the Rayleigh instability limit ($X = 1$) pertains to nuclear fusion induced by Coulomb explosion of homonuclear and heteronuclear deuterium- or tritium-containing molecular clusters (37–40), e.g., $(D_2)_n$, $(DT)_{n/2}$, $(D_2O)_n$, $(DTO)_n$, $(CD_4)_n$ ($n = 400$–10^4), stripped of all their valence electrons by multielectron ionization in ultraintense laser fields ($I = 10^{16}$–10^{19} Wcm^{-2}). The high energies (E = 1–20 keV) of the D^+ or T^+ ions (d or t nuclei) resulting from the Coulomb explosion of an assembly of clusters fall in the energy domain of nuclear physics, driving dd or dt nuclear fusion. An alternative way to obtain high values of the fissibility parameter, which are far above the Rayleigh limit, involves the drastic decrease of E(surface). This was achieved in three-dimensional optical molasses (34), consisting of a cloud of low-density (10^{10}–10^{11} cm^{-3}), ultracold (T = 10–100 μK), neutral (Rb) atoms subjected to the radiative trapping force, which is equivalent to the interatomic Coulomb force, with an effective atomic charge $q \simeq 10^{-5}e$ (34). The restoring surface energy is vanishingly small, whereupon $X \gg 1$, even for these low values of q. The nuclear dynamics of optical molasses, transcendenting the Rayleigh limit, manifests an isotropic, radial, spatial expansion, in analogy with isotropic cluster Coulomb explosion (34). The time scales for the isotropic expansion of optical molasses [$\tau_M \simeq$ 1 ms for Rb (34)] and for cluster Coulomb explosion [$\tau_M \simeq 100$ fs for $(Xe^+)_n$ (27)] differ by a numerical factor of 10^{10}, in accord with the theory of Coulomb explosion (34).

In the realm of biophysics, highly charged peptides and proteins in the gas phase are interrogated by mass spectrometry (41, 42), providing significant information on the structure, reactivity, conformational changes, and folding of "isolated" anhydrous proteins (41). It is interesting to inquire whether charged isolated protein fission or Coulomb explosion can be realized. Typical protein sizes (specified in terms of the number, n, of residues) and total charges (Z) currently available correspond to rather low values of Z^2/n, e.g., for cytochrome C (41), $Z = 8$–19, $n = 104$ ($Z^2/n \simeq 0.5$–4) and for carbonic anhydrase (41, 42), $Z = 45$, $n \simeq 260$ ($Z^2/n \simeq 7$), while for G-Actin (41) (with 46 basic residues) $Z = 59$, $n \simeq 370$ ($Z^2/n \simeq 9$). Adopting a very crude description of the Coulomb instability of globular proteins, these low values of $Z^2/n \simeq 1$–$10 \ll n$, together with large surface energies (i.e., $a \simeq 10^{-2}$–10^{-3}), imply that the fissibility parameter for these charged gas phase proteins is low, i.e., $X \ll 1$. Accordingly, only thermally activated protein fission over high barriers may be manifested, insuring the structural integrity of the charged protein in the mass-spectrometric experiments. Kinetic energy release studies (41, 42) of the melittin peptide ($Z = 3$, $n = 26$) reveal energetic ionic dissociation ($\Delta E = 1.25$ eV) of small fragments, presumably induced by local Coulomb effects. Further experimental and computational studies of Coulomb instability of highly charged proteins are called for.

We thank Professor Chava Lifschitz for stimulating discussions, Dr. Claude Guet for inspiring correspondence, and Professor Thomas Leisner for prepublication information. This research was supported by the James–Franck German–Israeli Binational Program on Laser–Matter Interaction.

1. Bohr, N. & Wheeler, J. A. (1939) *Phys. Rev.* **56,** 426–450.
2. Meitner, L. & Frisch, O. R. (1939) *Nature (London)* **143,** 239–240.
3. Frenker, S. & Metropolis, N. (1947) *Phys. Rev.* **72,** 914–925.
4. Möller, P., Madland, D. G., Sierk, A. J. & Iwamoto, A. (2001) *Nature (London)* **409,** 785–790.
5. Sattler, K., Muhlbach, J., Echt, O., Pfau, P. & Recknagel, E. (1981) *Phys. Rev. Lett.* **47,** 160–164.
6. Bréchignac, C., Cahuzac, Ph., Carliez, F. & de Frutos, M. (1990) *Phys. Rev. Lett.* **64,** 2893–2896.
7. Bréchignac, C., Cahuzac, Ph., Kebaili, N., Leignier, J. & Sarfati, A. (1992) *Phys. Rev. Lett.* **68,** 3916–3919.
8. Chandezon, F., Guet, C., Huber, B. A., Jalabert, M., Maurel, E., Monnand, E., Ristori, C. & Rocco, J. C. (1995) *Phys. Rev. Lett.* **74,** 3784–3787.
9. Bréchignac, C., Cahuzac, Ph., de Frotos, M., Kebaili, N. & Sarfati, A. (1996) *Phys. Rev. Lett.* **77,** 251–254.
10. Näher, U., Bjornholm, S., Fraundorf, S., Gracias, F. & Guet, C. (1997) *Phys. Rep.* **285,** 245–322.
11. Guet, C., Biquard, X., Blaise, P., Blundell, S. A., Gross, M., Huber, B. A., Jalabert, D., Maurel, M., Plague, L. & Rocco, J. C. (1997) *Z. Phys. D* **40,** 317–322.
12. Shapiro, O., Kunz, P. J., Möhring, K., Hervieux, P. A., Gross, D. H. F. & Madjet, M. E. (1997) *Z. Phys. D* **41,** 219–227.
13. Bréchignac, E., Cahuzac, Ph., Kebaili, N. & Leygnier, J. (1998) *Phys. Rev. Lett.* **81,** 4612–4615.
14. Daligault, J. & Guet, C. (2001) *Phys. Rev. A* **64,** 043203-1–043203-5.
15. Chandezon, F., Tomita, S., Cornier, D., Grubling, P., Guet, C., Lebius, H., Pesnelle, A. & Huber, B. A. (2001) *Phys. Rev. Lett.* **87,** 153402-1–153402-4.
16. Chandezon, F., Bergen, T., Brenac, A., Guet, C., Huber, B. A., Lebius, H. & Pesnelle, A. (2001) *Phys. Rev. A* **63,** 051201-1–051201-4.

17. Purnell, J., Snyder, E. M., Wei, S. & Castleman, A. W., Jr. (1994) *Chem. Phys. Lett.* **229,** 333–339.
18. Ditmire, T., Donnelly, T., Rubenchik, A. M., Falcone, R. W. & Perry, M. D. (1996) *Phys. Rev. A* **53,** 3379–3402.
19. Ditmire, T., Tisch, J. W. G., Springate, E., Mason, M. B., Hay, N., Smith, R. A., Marangos, J. & Hutchinson, M. H. R. (1997) *Nature (London)* **386,** 54–56.
20. Ditmire, T., Tisch, J. W. G., Springate, E., Mason, M. B., Hay, N., Marangos, J. P. & Hutchinson, M. H. R. (1997) *Phys. Rev. Lett.* **78,** 2732–2735.
21. Hutchinson, M. H. R., Ditmire, T., Springate, E., Tisch, J. W. G., Shao, Y. L., Mason, M. B., Hay, N. & Marangos, J. P. (1998) *Philos. Trans. R. Soc. London A* **356,** 297–315.
22. Ditmire, T., Springate, E., Tisch, J. W. G., Shao, Y. L., Mason, M. B., Hay, N., Marangos, J. P. & Hutchinson, M. H. R. (1998) *Phys. Rev. A* **57,** 369–382.
23. Springate, E., Hay, N., Tisch, J. W. G., Mason, M. B., Ditmire, G., Hutchinson, M. H. R. & Marangos, J. P. (2000) *Phys. Rev. A* **61,** 063201-1–063201-7.
24. Kou, J., Nakashima, N., Sakabe, S., Kawato, S., Ueyama, H., Urano, T., Kuge, T., Izawa, Y. & Kato, Y. (1998) *Chem. Phys. Lett.* **289,** 334–337.
25. Card, D. A., Wisniewski, E. S., Folmer, D. E. & Castleman, A. W., Jr. (2002) *J. Chem. Phys.* **116,** 3554–3567.
26. Lezius, M., Dobosh, S., Normand, D. & Schmidt, M. (1998) *Phys. Rev. Lett.* **80,** 261–264.
27. Last, I., Schek, I. & Jortner, J. (1997) *J. Chem. Phys.* **107,** 6685–6692.
28. Last, I. & Jortner, J. (1999) *Phys. Rev. A* **60,** 2215–2221.
29. Last, I. & Jortner, J. (2000) *Phys. Rev. A* **62,** 013201-1–013201-9.
30. Lord Rayleigh, L. (1882) *Phil. Mag.* **14,** 184–186.
31. Taflin, D. C., Ward, T. I. & Davis, E. J. (1989) *Langmuir* **5,** 376–384.
32. Widman, J. F., Arrdahl, C. L. & Davis, E. J. (1997) *Aerosol Sci. Technol.* **27,** 636–648.
33. Gomez, I. A. & Tang, K. (1993) *Phys. Fluids* **6,** 404–409.
34. Pruvost, L., Serre, I., Duong, H. T. & Jortner, J. (2000) *Phys. Rev. A* **61,** 053408-1–053408-9.
35. Berry, R. S. (1999) in *Theory of Atomic and Molecular Clusters*, ed. Jellinek, J. (Springer, Berlin), pp. 1–26.
36. Oganessian, Y. T., Yeremin, A. V., Popeko, A. G., Bogomolov, S. L., Buklanov, G. V., Chelnokov, M. L., Chepigin, V. I., Gikal, B. N., Gorshkov, V. A., Gulbekian, G. G., *et al.* (1999) *Nature (London)* **400,** 242–245.
37. Zweiback, J., Smith, R. A., Cowan, T. E., Hays, G., Wharton, K. B., Yanovsky, V. P. & Ditmire, T. (2000) *Phys. Rev. Lett.* **84,** 2634–2637.
38. Zweiback, J., Cowan, T. E., Smith, R. A., Hurtlay, J. H., Howell, R., Steinke, C. A., Hays, G., Wharton, K. B., Krane, J. K. & Ditmire, T. (2000) *Phys. Rev. Lett.* **85,** 3640–3641.
39. Last, I. & Jortner, J. (2001) *Phys. Rev. Lett.* **87,** 033401-1–033401-4.
40. Last, I. & Jortner, J. (2001) *Phys. Rev. A* **64,** 063201-1–063201-11.
41. Cherokee, S., Hoaglund-Hyzer, A., Counterman, E. & Clemmer, D. E. (1999) *Chem. Rev.* **99,** 3037–3079.
42. Laskin, J. & Lifshitz, C. (2001) *J. Mass Spectrom.* **36,** 459–478.